THE ASTROPHYSICAL JOURNAL, 428:599–608, 1994 June 20

NONTHERMAL PAIR MODELS, REFLECTION, AND X-RAY SPECTRAL VARIABILITY OF ACTIVE GALAXIES

P. GRANDI,[1] C. DONE,[2] AND C. M. URRY[1]
Received 1993 June 28; accepted 1993 December 22

ABSTRACT

Standard nonthermal electron-positron pair cascades, including the effects of reflection from an accretion disk, can explain reasonably well the mean spectra of low-luminosity, Seyfert-type active galaxies. We test this model using the spectral variability observed by *EXOSAT* between 0.05 and 10 keV in five active galaxies: NGC 5548, 3C 120, 3C 273, NGC 7469, and MCG 2-58-22. We find that pair-reflection models fail to reproduce the full range of spectra observed, particularly very hard spectra with a strong soft X-ray excess. Either the pair-reflection model is not an accurate description of the emission process in these objects or extrinsic effects, such as enhancement of the reflection component and/or a partially ionized absorber with a large column density, are responsible for much of the observed spectral variability.

Subject headings: accretion, accretion disks — galaxies: active — galaxies: Seyfert — X-rays: galaxies

1. INTRODUCTION

The *Einstein*, *EXOSAT*, and *Ginga* X-ray satellites have revealed a wealth of information about spectral and variability properties of active galactic nuclei (AGNs). The X-ray spectra can be characterized by a power-law spectrum plus features associated with Fe Kα in emission ($\sim$6.4 keV) and absorption (7–9 keV) and an excess over this power law at hard ($\geq$ 8 keV) and soft ($\leq$ 1 keV) energies (Arnaud et al. 1986; Wilkes & Elvis 1987; Turner & Pounds 1989; Kruper, Urry, & Canizares 1990; Urry et al. 1989; Piro, Yamauchi, & Matsuoka 1990; Pounds et al. 1990). The X-ray spectral features are particularly exciting because they can be produced by cold, optically thick matter subtending a large solid angle to the X-ray source, providing some of the best evidence to date for presence of an accretion disk in AGNs. Compton reflection from the surface of the X-ray illuminated disk can produce the iron line and hard excess (Guilbert & Rees 1988; Lightman & White 1988), while thermal emission from the same material can produce the soft excess (e.g., Laor 1990; Ross & Fabian 1993 and references therein); meanwhile, the underlying photon index of the intrinsic power-law emission is $\Gamma \sim 1.9$ (e.g., Pounds et al. 1990).

The rapid X-ray variability observed in many AGNs (McHardy 1989; Grandi et al. 1992, hereafter G92) implies a very small size scale for the X-ray region and, coupled with the high X-ray luminosity, a very high photon density in both hard and soft X-rays. The radiating electrons then probably cool by inverse Compton scattering of the soft X-ray excess emission. However, electron-position pair production can be an important modification to the emission, as the hard X-ray photon density is such that any γ-rays produced in the source have a high probability of interacting in photon-photon collisions (Lightman & Zdziarski 1987; Done & Fabian 1989).

Recent models based on this inverse Compton/pair production scenario have had considerable success in reproducing the X-ray emission from AGNs (Zdziarski et al. 1990a). So-called "standard" pair models use relativistic electrons to inverse Compton scatter the copious UV-soft X-ray photons, producing a spectrum extending up to γ-ray energies. The γ-rays interact with X-ray photons to create electron-positron pairs ($e^{\pm}$), which, in turn, inverse Compton scatter the soft photons in a pair cascade that saturates to a photon index of $\Gamma \sim 2$ (Svensson 1987). Once cooled, the pairs can further modify the spectrum through thermal Compton upscattering of the soft photons to produce a soft X-ray excess (Zdziarski & Coppi 1991). Such models have been studied extensively in recent years (Guilbert, Fabian, & Rees 1983; Zdziarski & Lightman 1985; Zdziarski 1986; Fabian et al. 1986; Svensson 1987; Lightman & Zdziarski 1987; Done & Fabian 1989; Svensson 1991). In order to match the observed AGNs spectra, particularly the iron emission line and the 10 keV excess, part of the X-ray flux emerging from the pair source must be intercepted by an accretion disk and reprocessed into a Compton reflection spectrum and fluorescent iron line.

Such models provide an attractive explanation of AGNs spectra, producing both the mean observed spectral index and the soft excess. However, detailed spectral tests of the three AGNs with the best determined high-energy spectra, NGC 4151, 3C 273 and Cen A, have produced conflicting results, possibly because these are not "typical" low-luminosity Seyfert-type AGNs as described above. Both 3C 273 and Cen A are radio-loud, and so may well have nuclear X-ray emission which is contaminated by a relativistic jet, while NGC 4151, though classified as a radio-quiet Seyfert galaxy, has an unusually flat X-ray spectral index of $\Gamma \leq 1.5$ (Yaqoob & Warwick 1991) and no reflection component (Maisack & Yaqoob 1991; Yaqoob et al. 1993). In the context of nonthermal pair models, such flat spectral indices can be produced if the UV photon density is smaller than that of the hard X-rays, the so-called "photon-starved" state (Zdziarski, Coppi, & Lamb 1990b). The X-ray spectral variability of NGC 4251 (Yaqoob 1992) and its broad-band X–γ-ray spectrum as determined by the ART-P and SIGMA instruments on the *Granat* satellite (Coppi & Zdziarski 1992) can be interpreted in these photon-starved pair models, although these predict too strong an annihilation line and too flat an X-ray spectrum compared to the hard X-ray spectrum observed with the OSSE instrument on the *Compton GRO* satellite (Maisack et al. 1993; Zdziarski et al. 1993). The only "typical" AGN for which the

[1] Space Telescope Science Institute, 3700 San Martin Drive, Baltimore, MD 21218.
[2] Department of Physics and Astronomy, University of Leicester, University Road, Leicester, LE1 7RH, England, UK.

pair-reflection models have been tested is Mrk 335, where the 0.4–20 keV spectrum observed with *Ginga* and BBXRT can be well described in the "standard" pair cascade models (Turner et al. 1993).

Here we use the recent study of spectral variability of AGNs observed with *EXOSAT* (G92) to test the pair-reflection models on a much larger sample of objects. The X-ray data with the highest signal-to-noise ratio, which inspired the reflection model in the first place, were from the *Ginga* satellite, which was not sensitive below ~ 1.5 keV. Thus, applying the pair-reflection model to the *EXOSAT* data, with its sensitivity to photons a factor of 30 lower in energy, offers an excellent test of the true applicability of the model. We characterize the spectral shape in terms of two hardness ratios: $HR_{\rm ME}$, the ratio between the 6–10 keV and 3–6 keV counts, and $HR_{\rm ME/LE}$, the ratio between the 1–8 keV and the 0.05–2 keV counts. The former carries information about changes in the hard part (3–10 keV) of the AGNs spectra, while the latter is also sensitive to the soft photon variations. We find that despite the wide range of input parameters investigated, some observed spectral variability cannot be reproduced by pair-reflection models. Specifically, hard spectra ($\Gamma \leq 1.5$) with soft excesses, an occasional state of most of the AGNs we studied, cannot be produced by pair-reflection models. Hard spectra can be made only in the photon-starved regime, which is characterized by a low ratio of soft X-ray luminosity to luminosity of injected relativistic electrons, but in these models the hard spectra are obtained by multiple Compton scatterings of the soft photons, so that no soft excess remains. It is possible that these hard/soft spectra can be produced by external effects, such as strong enhancement of the reflection component, soft thermal emission from the accretion disk (perhaps reprocessed hard X-rays) that is not intercepted by the hard X-ray source, and/or the presence of a partially ionized absorber, but in these cases the spectral shape and variability cannot be used as a diagnostic of the intrinsic source emission mechanism. In other words, an additional component is required: the static pair-reflection models that fit the mean X-ray spectra of low-luminosity Seyfert-type AGNs predict significantly different X-ray variability than is observed.

A brief description of the studied AGNs is given in § 2. Model assumptions and the theoretical hardness ratios computation are outlined in § 3. The results of comparing data to theory are shown in § 4. General discussion and conclusions are respectively given in §§ 5 and 6.

2. THE STUDIED AGNs AND THEIR X-RAY SPECTRAL CHARACTERISTICS

Five AGNs were chosen to test the pair-reflected model: NGC 5548, NGC 7469, MCG 2-58-22, 3C 120, and 3C 273. They belong to the spectral survey of G92 and were selected because they show significant spectral variability in both $HR_{\rm ME}$ and $HR_{\rm ME/LE}$ but no evidence for intrinsic cold absorption above the Galactic column density (which could potentially confuse the analysis). The first three are Seyfert type 1 galaxies, 3C 120 is a broad-line radio galaxy (the radio-loud equivalent of a Seyfert 1), and 3C 273 is a radio-loud quasar which sometimes exhibits optically violent variable (OVV) characteristics. The X-ray continuum from the two radio-loud objects, especially 3C 273, may be contaminated by a blazar component, such as beamed emission from a relativistic jet.

Spectral fits using *EXOSAT* and *Ginga* data have shown that all the Seyfert 1 galaxies in this sample have an emission line and a hard excess at 10 keV, and that all but MCG 2-58-22 show evidence for a soft X-ray excess (Barr 1986; Kaastra & Barr 1989; Turner & Pounds 1989; Pounds et al. 1989; Piro et al. 1990; Walter & Courvoisier 1990; Nandra et al. 1991b). This makes them very good candidates on which to test the pair-reflection model. 3C 120 was not observed with *Ginga*, so there are no strong constraints on the presence of the hard tail or iron line, and there is no evidence from *EXOSAT* of a soft excess (Turner & Pounds 1989; Maraschi et al. 1991). In contrast, 3C 273 has been extensively studied and shows a strong soft excess below 2 keV in *Einstein*, *EXOSAT*, and *ROSAT* data (Wilkes & Elvis 1987; Turner & Pounds 1989; Courvoisier & Camenzind 1989; Staubert et al. 1991). The many *Ginga* spectra of 3C 273 confirm the presence of the iron emission line (Turner et al. 1990) previously detected with the *HEAO 1* A-2 experiment (Worrall et al. 1979). Although the iron line suggests that cold matter lies near the continuum source, few of the *Ginga* observations of 3C 273 allow significant amounts of reflection (Williams et al. 1992), suggesting that the line may be from the X-ray illuminated broad-line region rather than from the accretion disk (Turner et al. 1993).

3. PHYSICAL ASSUMPTIONS AND COMPUTATION OF HARDNESS RATIOS

We use a detailed pair-production model to produce the primary continuum radiation, which corresponds roughly to a power law. We then calculate the effects of reflection of some fraction of the continuum, under a variety of geometric assumptions. The final spectrum used to calculate *EXOSAT* hardness ratios is the sum of the direct and reflected components. Here we describe the assumptions inherent in the pair-production model and the reflection model.

Our standard pair-production models assume that in a homogeneous region of size $R \sim 10^{15}$ cm a monoenergetic injection of primary particles at energy γ cool on a blackbody photon spectrum peaked at UV energy x_s (where $x_s = 2.8kT_{\rm bb}/m_e c^2$, $T_{\rm bb}$ being the blackbody temperature). As the blackbody emission is assumed to be produced in the inner regions of the accretion disk it has a typical temperature of 5–50 eV, or $x_s = 10^{-5}$ to 10^{-4}, and it is assumed that all these inner disk photons are intercepted by the electron source. The shape of the injected electron spectrum can be quite unimportant in determining the resultant X-ray spectrum. For an injection rate $\propto \gamma^{-s}$ for $1 \leq \gamma \leq \gamma_{\rm max}$, where γ is the electron Lorentz factor, the X-ray spectrum is similar to that from monoenergetic injection if $s \ll 2$ (Kazanas 1984; Zdziarski & Lightman 1985). The standard pair models use this fact to add to the robustness of the derived results; alternative models with steep electron spectra ($s \geq 2$, for which the X-rays are affected by the initial injection) are not considered. The relativistic electron (L_h) and soft photon (L_s) luminosities are measured in terms of the dimensionless compactness parameters l_h and l_s, defined as $l = L/R\ (\sigma_{\rm T}/m_e c^3)$, where $\sigma_{\rm T}$ is the Thomson scattering cross section.

The energetic electrons cool by inverse Compton scattering of the blackbody photons, boosting them in energy by a factor $\sim \gamma^2$. Thus γ-rays are produced if $\gamma \gtrsim x_s^{-1/2}$ (here $x_s \leq 10^{-4}$, so $\gamma \geq 100$ gives substantial γ-ray emission). The γ-rays can interact with lower energy photons to create electron-position pairs, which also cool by inverse Compton scattering the photon distribution. In order to have more than one pair generation, it is necessary for the created pairs to themselves reradiate γ-rays, which results on a condition on the initial

injection of $\gamma \sim x_s^{-3/4}$($\gamma \gtrsim 10^3$ for $x_s \leq 10^{-4}$). The calculations assume that the scattering takes place in the Thomson regime i.e., $\gamma x_s \leq 1$. This is not an important restriction as Zdziarski (1988) showed that cascades in the Klein-Nishima range, where $\gamma x_s \geq 1$, are well described by the equivalent Thomson cascade replacing γ by $1/x_s$.

Once the injected particles and the created electron-positron pairs have cooled down to the equilibrium temperature with the radiation field, they can further distort the spectrum. Thermal downscattering of hard photons imprints a high-energy break in the spectrum for $\tau_T \geq 1$ (τ_T being the Thomson optical depth of the thermal pairs). The exact position and strength of the break are a function of the distribution of photons and pairs within the source; simple considerations show that the characteristic break energy is $E_{\rm break} \sim (511\ {\rm keV})/\tau_T^2$, while detailed calculations show the break can be up to a factor 2–3 higher in energy (Sunyaev & Titarchuk 1980; Pozdnyakov, Sobol, & Sunyaev 1983). Thermal Compton upscattering can also play a marked role in the spectrum, boosting the soft blackbody photons to produce a steep power at low energies, $\epsilon < kT_{\rm pair}$, where $T_{\rm pair}$ is the equilibrium temperature of the thermal pair plasma. However, excess soft photons are available only for thermal Compton upscattering if $l_s/l_h \gtrsim 1$; in "photon-starved" sources, where $l_s/l_h \lesssim 1$, all the soft photons are used up in the relativistic scatterings (Zdziarski, Coppi, & Lamb 1990b).

Thermal Comptonization becomes saturated when the Compton y-parameter, $y \sim 4\tau_T^2 kT_{\rm pair}/m_e c^2$, gets larger than 1. This rarely happens in spectra with $l_s/l_h \geq 1$ because the electrons interact with the many cool blackbody photons and thermalize at low temperature. However, in photon-starved sources, the blackbody is no longer the dominant radiation field, so the equilibrium temperature, $kT_{\rm pairs}$, is much higher. Then the thermal Compton scattering can saturate, so that the spectrum is dominated by a Wien hump at energy $\epsilon \sim kT_{\rm pair}$.

The pair-plasma spectrum emerges isotropically from the continuum source, illuminating an accretion disk to produce a Compton reflection spectrum (Guilbert & Rees 1988; Lightman & White 1988; White, Lightman, & Zdziarski 1988). The reflected spectrum differs from the incident spectrum because of the effects of photoelectric absorption at low energies and Compton downscattering at high energies. The reflected photons come from all radii of the disk: assuming a flat, face-on geometry, half of the reflected photons come from outside 20 Schwarzschild radii (Matt, Perola, & Piro 1991). The photons that are intercepted by the disk but not reflected are absorbed and are either reemitted as an Fe Kα line or thermalize at the local blackbody temperature. Thus the thermalized photons are generally at a much lower temperature than the inner disk photons, so we assume that their contribution to the soft X-ray spectrum is negligible. Detailed discussion of the continuum and emission-line structure of the reflected spectra can be found in George & Fabian (1991) and Matt et al. (1991), while the thermalized spectrum is discussed in Ross & Fabian (1993).

The nonthermal region producing the incident pair spectrum is assumed to be located near the accretion disk, and we use the method of Lightman & White (1988) to calculate the shape of the reflected spectrum assuming that the disk is unionized. This component is then normalized to the mean angle-integrated reflection spectrum, and so is appropriate for a disk viewed at $\sim 60°$. We term this normalization $N_{\rm refl} = 1$, and for a face-on accretion disk the normalization is boosted by a factor ~ 1.5 (Haardt 1993). We have used these two normalizations as the expected extremes of the reflection component, which match well with the measured reflection contribution from detailed spectral analysis of individual *Ginga* spectra (Piro et al. 1990; Nandra et al. 1991b; Fiore et al. 1992). Although the presence of the iron emission line changes the $HR_{\rm ME}$ values by only a few percent, we added this feature to the synthetic spectra of NGC 5548, NGC 7469, and MCG 2-58-28 to be consistent with the observations (Leighly, Pounds, & Turner 1989; Nandra et al. 1991a). No emission line was added to theoretical spectra of 3C 273 because of its very weak emission line (EW $\sim$ 50 eV; Turner et al. 1990).

Once computed, the pair-reflection spectra are modified by absorption by a uniform column density of cold material with solar abundances (parameterized by the Galactic column density of hydrogen, $N_{\rm H}$; Stark et al. 1992), and folded through the response curves of the *EXOSAT* LE (0.05–2 keV) and ME (1–15 keV) instruments. In order to convert these theoretical spectra to instrumental counts rates for comparison with the observational data, hardness ratios for the 6–10 keV/3–6 keV ($HR_{\rm ME}$) and 1–8 keV/0.05–2 keV ($HR_{\rm ME/LE}$) bands are calculated for the final simulated spectra using the XSPEC package (XSPEC-*EXOSAT* Database: User Guide 1991).

4. COMPARISON TO OBSERVATIONS

In calculating pair-reflection spectra, we explored a wide range in parameter space, spanning the values typically used to explain individual high-quality *Ginga* spectra. The discrete values used were

$l_s/l_h = [0.01, 0.1, 1, 10]$,
$l_h = [0.1, 0.2, 0.4, 0.9, 1, 2, 4, 9, 10, 20, 40, 90, 100, 200]$,
$\gamma_{\rm max} = [10^3, 10^4]$,
$x_s = [10^{-5}, 10^{-4}]$,
$N_{\rm refl} = [1.0, 1.5]$.

Four grids of incident pair spectra were computed for each reflection normalization, fixing the peak energy of the blackbody (x_s) and the Lorentz factor for the primary electron injection ($\gamma_{\rm max}$) while varying the hard (l_h) and the soft to hard (l_s/l_h) compactness.

4.1. *Predicted Spectral Variations*

We illustrate the spectral variations predicted by the pair-reflection models using two grids of models with same Lorentz factor, $\gamma_{\rm max} = 10^3$, but different blackbody temperatures. $HR_{\rm ME/LE}$ ratios are plotted against $HR_{\rm ME}$ ratios for the two different values of x_s in Figure 1. Different symbols indicate theoretical ratios for different values of the l_s/l_h input parameters (as described in the figure caption) and lines represent the tracks for l_h increasing from 0.1 to 200. In both cases, the accretion disk is assumed to be face-on and the Galactic column density $N_{\rm H} = 1.6 \times 10^{20}$ cm^{-2}. The evolution tracks of models with $\gamma = 10^4$ occupy a slightly different region of the hardness ratios plot, but the predicted spectral variations are qualitatively the same.

In general, higher soft-to-hard compactness ratios imply softer spectra; i.e., models with higher values of l_s/l_h are characterized by lower $HR_{\rm ME/LE}$. For a fixed value of l_s/l_h, increasing the hard compactness leads to more pair-reprocessing of the γ-rays into the X-ray band, so increasing l_h leads to progressively steeper ME spectra and to decreasing $HR_{\rm ME}$. For photon-starved plasmas ($l_s/l_h < 1$), however, the equilibrium temperature is high, $kT_{\rm pair} \gg kT_{\rm bb}$, and the pair yield (PY) is

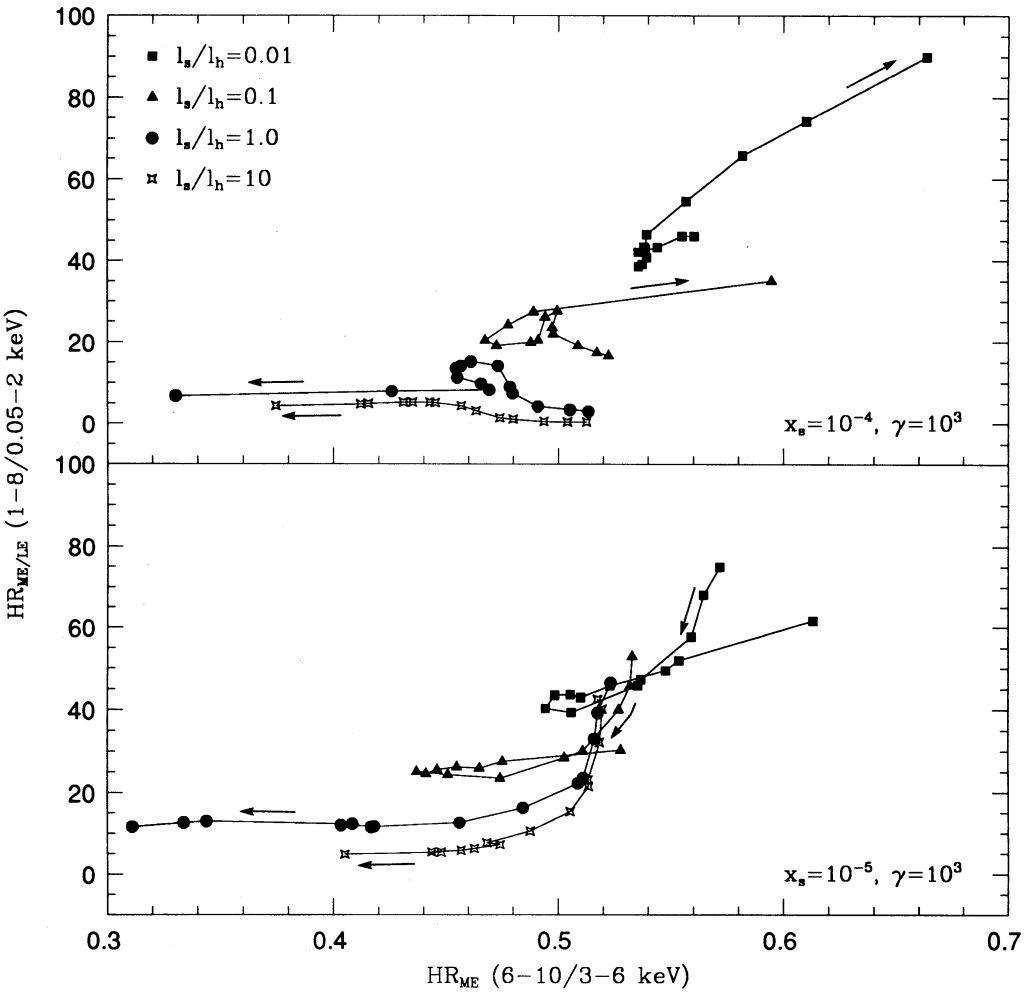

FIG. 1.—Hardness ratios from combined nonthermal pair and reflection models are shown for the input parameters $x_s = 10^{-4}$, $\gamma_{max} = 10^3$ (*top panel*); $x_s = 10^{-5}$, $\gamma_{max} = 10^3$ (*bottom panel*). In each diagram the lines connect points with same l_s/l_h and l_h from 0.1 to 200 (increasing in the direction of the arrows). The column density assumed is $N_H = 1.6 \times 10^{20}$ cm^{-2} and the disk face-on.

also boosted by a factor of ~ 2 (Done, Ghisellini, & Fabian 1990) so that the optical depth $\tau_T \propto (l_h \mathrm{PY})^{1/2}$ is also larger. The Compton y-parameter can then be ≥ 1, leading to a Wien peak in the spectrum and to spectral hardening. Thus with increasing l_h the photon-starved models move toward lower HR_{ME} and $HR_{ME/LE}$ as pair production steepens the spectrum, and then move to higher HR_{ME} and $HR_{ME/LE}$ as the thermal Wien peak becomes strong enough to harden the spectrum.

For $l_s/l_h \geq 1$, the ME/LE hardness ratio changes depend strongly on the blackbody temperature of the accretion disk. For low compactnesses, where pair-reprocessing is negligible, the higher blackbody temperature gives rise to a much higher LE flux, and so to a much lower $HR_{ME/LE}$. As the compactness increases, the pair-reprocessing starts to affect the spectrum. The pair reradiation affects only the LE flux if $x_s = 10^{-5}$, but affects both the LE and the ME if $x_s = 10^{-4}$. Thus for a low blackbody temperature the pair reprocessing acts as an additional soft LE component, decreasing $HR_{ME/LE}$ for increasing compactness. For a higher blackbody temperature, the pair reprocessing increases the ME flux relative to the LE flux, as the latter is already dominated by the blackbody emission. Thus with $x_s = 10^{-4}$ and $\gamma = 10^3$, $HR_{ME/LE}$ increases with compactness; however, this stops when the spectrum becomes saturated (when every γ-ray photon produces a pair), after which the ratio between soft and hard counts remains almost constant.

The reflection component always tends to harden the spectrum and its effects are stronger for larger amounts of reflection. Geometries with a face-on disk produce a stronger reflection continuum than those where the disk is viewed at an angle.

4.2. *Models versus Data*

In Figures 2–6, the X-ray spectral data (*filled circles*) are compared to a shaded area that spans all the theoretical hardness ratios for a given N_{ref}. Each diagram looks different because N_H is different. A brief discussion of the results for each AGN is given below.

NGC 5548.—NGC 5548 shows the most common spectral behavior observed in the Seyfert galaxies. As revealed by both *EXOSAT* and *Ginga* observations, this source becomes softer when the luminosity increases (Branduardi-Raymont 1989; Walter & Courvoisier 1990; Nandra et al. 1993; G92). The comparison between data and models (Fig. 2) reveals the difficulty the pair-reflections models have in reproducing the hardest HR_{ME} spectra.

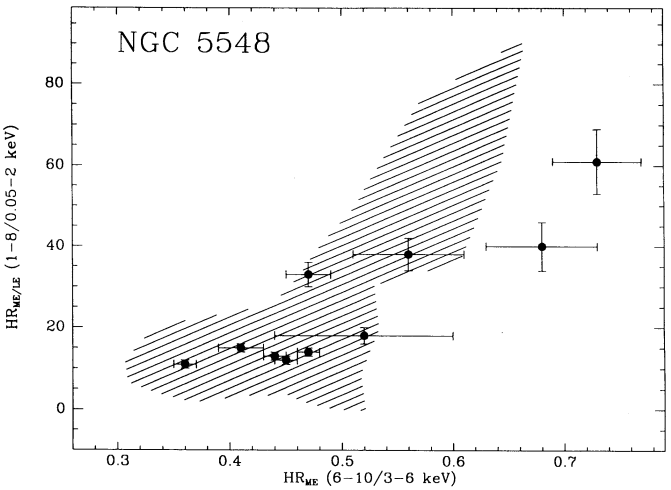

FIG. 2.—Observed hardness ratios (*filled circles*) of NGC 5548. The shaded region includes the hardness ratios produced by all the studied models (l_s/l_h = [0.01, 0.1, 1, 10], l_h = [0.1, 0.2, 0.4, 0.9, 1, 2, 4, 9, 10, 20, 40, 90, 100, 200], γ_{max} = [10^3, 10^4], x_s = [10^{-5}, 10^{-4}]) assuming $N_H = 1.6 \times 10^{20}$ cm^{-2} and the accretion disk face-on.

NGC 7469.—NGC 7469 is characterized by a complex spectral variability, with the spectrum hardening when the 1–8 keV flux increases and the 0.05–2 keV flux decreases (Barr 1986; G92). Although this behavior is qualitatively explained by the theoretical variations of photon-starved models (which predict a spectral hardening at the expense of the soft excess), the comparison between data and theory shows that very high HR_{ME} are again outside the model predictions (see Fig. 3).

MCG 2-58-22.—MCG 2-58-22 is a source with spectral variations very similar to NGC 5548. In this case, the pair-reflection models do encompass the observed spectral variability, as MCG 2-58-22 did not show hard spectra ($HR_{ME} \geq 0.5$), or indeed a large range in spectral variability, during the *EXOSAT* observations (Fig. 4). The grid of models which fit these data reasonably well have $x_s = 10^{-4}$, γ_{max} = [10^3, 10^4], and disk illumination at 60° inclination. Changes in both l_s/l_h (from 1 to 10) and in the input electron luminosity (by a factor

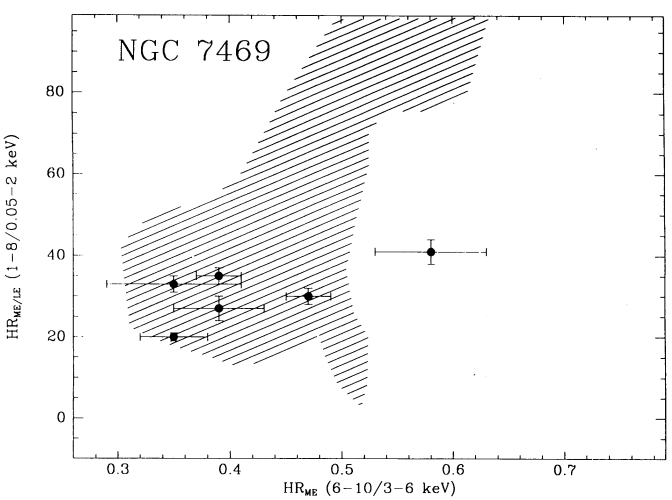

FIG. 3.—Observed hardness ratios (*filled circles*) of NGC 7469. As in the previous figure the shaded lines delimit the region of the theoretical hardness ratios (as in Fig. 2). Here N_H is 4.9×10^{20} cm^{-2} and the accretion disk is face-on.

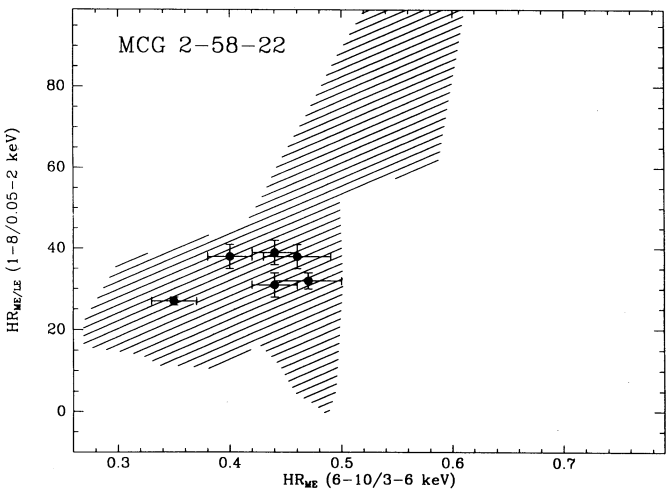

FIG. 4.—Observed hardness ratios of MCG 2-58-22 (*filled circles*) are within the region (*shaded lines*) spanned by the theoretical hardness ratios (as in Fig. 2). The synthetic spectra are computed for an accretion disk viewed at 60° and absorbed by the Galactic column density $N_H = 3.6 \times 10^{20}$ cm^{-2}.

100) can reproduce all the observations, but only the softest point in the plot represents a significant spectral change, so any conclusion about this object is not definitive.

3C 120.—The spectral variability of 3C 120 is similar to NGC 7469, although 3C 120 is a radio-loud object, with some blazar properties. As for NGC 7469, the pair-reflection models fail to reproduce the hardest X-ray spectrum observed in this source (Fig. 5).

3C 327.—As there are strict limits on the amount of reflection that can contribute to the spectrum of 3C 273, only models with the smallest amount of reflection ($N_{refl} = 1$) are used. 3C 273 is the object showing the most complex spectral behavior. Data collected from *Ginga* and *EXOSAT* observations showed that no clear trend can be found between the spectral variations and the luminosity (Williams et al. 1992; G92). In contrast to the previous sources, the theoretical hardness ratios do not match the two *softest* HR_{ME} of 3C 273 (Fig. 6). Most of the observations can be described by changing l_h between 2 and 200 and l_h/l_s between 0.1 and 1, but no input

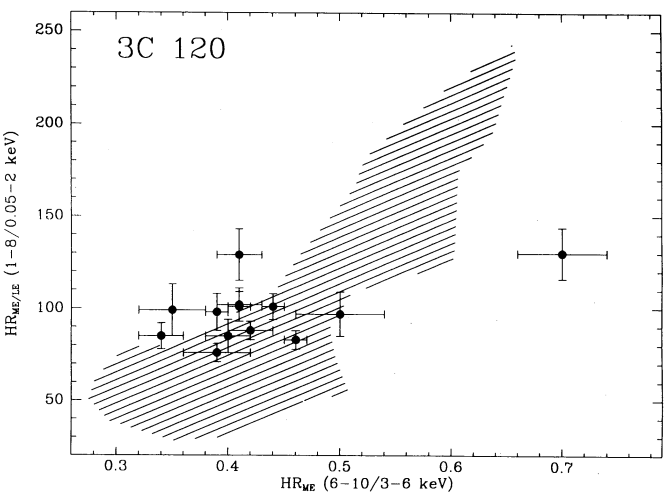

FIG. 5.—Hardness ratios of 3C 120 (*filled circles*) and region including theoretical hardness ratios (as in Fig. 2) for an accretion disk viewed face-on and $N_H = 1.0 \times 10^{21}$ cm^{-2}.

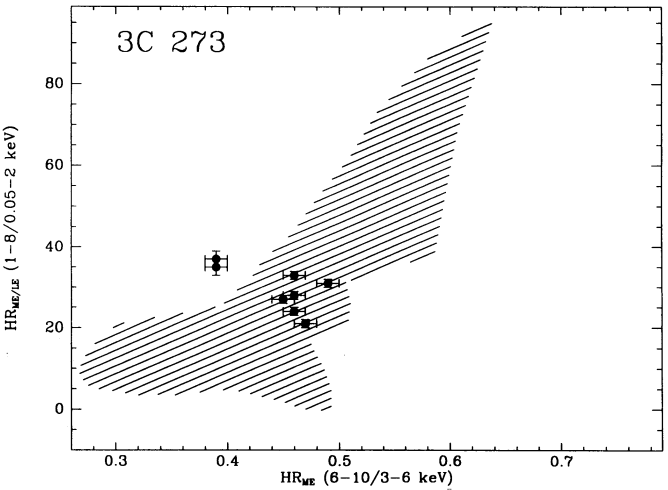

FIG. 6.—Observed hardness ratios of 3C 273 (*filled circles*). As in the previous figures, the shaded region includes all the hardness ratios computed for an accretion disk face-on. The Galactic column density in the direction of 3C 273 is $N_H = 1.8 \times 10^{20}$ cm^{-2}.

parameters can explain the data with the highest $HR_{ME/LE}$ values.

5. DISCUSSION

Despite the large range of parameter space investigated, the predicted spectral variations from a pair-reflection plasma generally do not match the *EXOSAT* data. The simplest type of variability, that of changing l_h in a model of constant l_s/l_h, γ, x_s, and N_{refl} cannot fit the observed spectral variability. Including changes in l_s/l_h increases the range of $HR_{ME/LE}$, but all the models predict a smaller range for HR_{ME} than is observed (compare Fig. 1 to Figs. 2, 3, and 5). Only for MCG 2-58-22 can the observed spectral variations be reproduced with values of the hard compactness ($2 < l_h < 200$) and the ratio of soft-to-hard luminosity ($1 < l_s/l_h < 10$) that are suggested in standard nonthermal pair-reflection models. For the other two radio-quiet objects and for 3C 120, the hardest spectra cannot be accounted for by pair-reflection models with any set of parameters in the extensive grid explored, while for 3C 273 it is the softest spectra that are not well fitted.

We now consider possible explanations for this discrepancy, both from the approximations used in the model and from external effects. The hardest spectra produced by pair-reflection models are dominated by thermal Comptonization. The pair code used here neglects dispersion effects, so the Wien peaks in these calculated spectra are too sharp. This leads to an *overestimate* of HR_{ME} if the Wien peak falls below 10 keV, or an *underestimate* of HR_{ME} for a Wien peak above 10 keV. Thus for photon-starved models of moderate compactness the spectral hardness is slightly underestimated. A comparison between our results and calculations that take the dispersion properly into account (S. P. Coppi, private communication) shows that there is rather good agreement for $l_s/l_h = 0.1$, but for the more extreme case where $l_s/l_h = 0.01$ our model does slightly underestimate HR_{ME}, as expected (see Table 1). However, even with the proper dispersion, the models are no closer to matching the hardest observed spectra than before.

It is possible that the data do not reflect stationary states. In pair models, the variability processes are essentially controlled by the light-crossing time, $t_c = R/c$, when $\tau_T < 1$, or by the escape time, $t_e = (1 + \tau_T)R/c$, when $\tau_T > 1$. Assuming $R = 10^{15}$ cm, it can then take from ~ 9 hr to few days for the compact source to change from one state to another (depending on the optical depth of the pairs). In the present case, observations for each source are generally several weeks apart and flux variations are detected within a single observation in very few cases, so comparing stationary states is reasonable. Among the poorly fitted hardness ratios, only the hardest point NGC 7469 could represent a transitional state.

Figure 7 illustrates the problem of the hard spectra in more detail, using the data from NGC 5548. The observed hardness ratios (*diamonds*) are shown together with the hardness ratios predicted by a simple power law of photon index between 1 and 2 (*solid line*), the same power laws with face-on reflection (*dotted line*) and again with reflection enhanced by an arbitrary factor $N_{refl} = 10$ (*dashed line*). Any soft excess will affect only the LE count rate and so move the theoretical points vertically on the plot. While the points below $HR_{ME} = 0.5$ can be fitted by an intrinsic power law with $\Gamma \geq 1.5$ plus reflection and a soft excess, those with $HR_{ME} \geq 0.5$ require either greatly enhanced reflection or spectra which are intrinsically flat, $\Gamma \leq 1.5$, together with the standard reflection component and soft excess.

NGC 5548 has both an extremely hard spectrum and a soft excess (hard spectra have low $HR_{ME/LE}$), so not even extreme pair plasmas with $l_s/l_h \ll 10^{-2}$ and/or $l_h \gg 200$ can reproduce the data. Hard spectra can be produced only from multiple Compton upscattering of the soft photons, but this effectively destroys any soft excess. The soft photons then have to be external to the hard X-ray source for any soft excess to survive, requiring a geometry in which only part of the hottest disk photons (whether they are produced intrinsically by viscous processes or by thermalization of the hard X-ray illuminating flux) are intercepted by the hard X-ray source.

The hardest HR_{ME} spectra of 3C 120 pose the same problem, again requiring inhomogeneous soft X-rays and an extreme pair-dominated source. The hardest point of NGC 7469 needs only a very strong reflection component and an external soft excess. The photon-starved model is not required in this case, because the hardness ratio reaches a value of only $HR_{ME} \sim 0.6$ and the slope of the X-ray spectrum is $\gamma \sim 1.8$, not particularly

TABLE 1

COMPARISON OF NGC 5548 HARDNESS RATIOS FROM DIFFERENT CODES

				Done Code		Coppi Code	
x_s	l_h[a]	N_{ref}	l_s/l_h	HR_{ME}	$HR_{ME/LE}$	HR_{ME}	$HR_{ME/LE}$
2.8×10^{-4}.....	48	1	0.01	0.56	71	0.60	82
2.8×10^{-4}.....	48	1	0.1	0.44	24	0.45	28

[a] Because of a difference of a factor $4\pi/3$ between the two codes, the l_h value actually used in the Coppi code is 200.

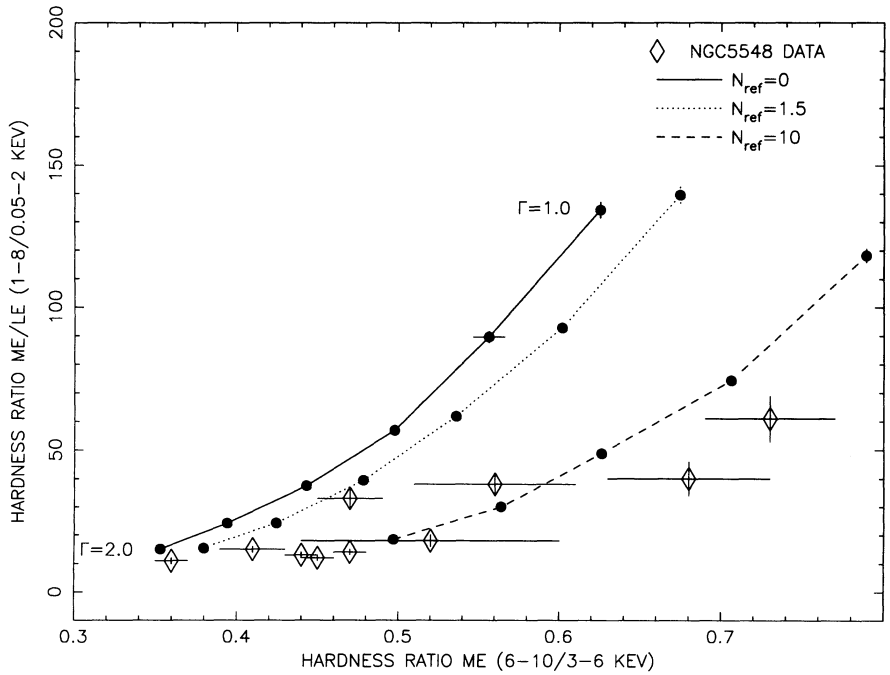

FIG. 7.—NGC 5548 data are compared to the hardness ratios predicted by simple power laws with photon indeces 1.0, 1.2, 1.4, 1.6, 1.8, 2.0 (*solid line*). The same power laws with face-on reflection N_{refl} (*dotted lines*) and with reflection increased by a factor $N_{refl} = 10$ (*dashed line*) are shown.

hard (compare Fig. 7 to Fig. 2). However, it should be stressed that the hardest point in the NGC 7469 plot corresponds to an observation showing short time variability (G92), so that the steady-state models may not be appropriate.

As Figure 7 suggests, hard spectra can be reproduced by enhancing the reflection component. However, our models already use the face-on case, which produces the maximum reflection component expected from flat, solar abundance disk. When the inclination angle increases (i.e., the disk goes from face-on to edge-on) the contribution from the reflection component diminishes and the spectrum becomes softer. If the disk were substantially underabundant in heavy elements, then the reflection component would be enhanced because the photoelectric absorption is less, but this seems unlikely as spiral galaxies show an increasing abundance toward the central regions (Pagel & Edmunds 1981). Enhancing the reflection through increasing the covering fraction of the disk gives at most a factor of 2 increase in the reflection normalization for an extreme funnel, which is not enough to produce the hardest spectra without still requiring an intrinsically hard spectrum and a soft excess (see Fig. 7).

The amount of reflection could be over or underestimated if our implicit assumption that the direct and reflected components vary together is not correct. This will be the case if the reflection region is much larger than $R = ct_{obs}$, where for typical ME-*EXOSAT* observation of $t_{obs} \sim 10^4$–10^5 s, i.e., $R \sim 3 \times 10^{14}$–10^{15} cm. Since reflection probably arises within 10–100 Schwarzschild radii (Matt et al. 1991), the reflection lag can be appreciable for a black hole mass larger than $10^8\ M_\odot$. However, a typical Seyfert black hole mass is probably $\sim 10^7\ M_\odot$ (Wandel & Mushotzky 1986), so a lag from reflection from the accretion disk should not be very important for our sources except the quasar 3C 273.

The time lag is probably more important if there is an *external* source of reflection other than the accretion disk, such as the putative molecular torus. The larger distance of the material ($\sim$ few pc) then means that there can be substantial discrepancies between the directly observed hard flux and its reflection from the torus when the X-ray source flux varies on timescales of years. If the hole of the torus has a half opening angle $\theta_{1/2} = 35°$ as in simple Seyfert 1 and 2 unification schemes (e.g., Lawrence 1991), then the material subtends a solid angle $\Omega/2\pi = 2 \cos \theta_{1/2} = 1.6$. If the accretion disk is still present, the total solid angle subtended by reflecting material (disk plus torus) in the upper half plane is $\Omega/2\pi = 1 + \cos \theta_{1/2} = 1.82$. That is, the torus contributes an additional 82% to the reflected flux from a flat accretion disk alone. In NGC 5548, the central source brightness decreases by a factor of 10 (G92), so the torus reflection could be $N_{refl} \sim 1.5 \times 0.82 \times \sim 10$–$12$, enough to produce the hardest spectra observed.

A strong reflection component may also be produced in a *single* pair-reflection source without invoking external components through the anisotropy of the Compton-scattered emission. If the soft photons are indeed emitted by an accretion disk, then the relativistic electrons lose more energy in head-on collisions, resulting in inverse Compton emission directed toward the disk, than in small-angle scatterings which direct inverse Compton emission spectrum away from the disk (Ghisellini et al. 1991; Rogers 1991). The magnitude of this effect depends on the directional pattern of accretion disk radiation, which in turn depends on general relativistic effects at the inner edge of the disk, deviations from flatness due to heating, and other effects that are not well-constrained in current accretion disk models. Nevertheless, a rough calculation shows that for large γ, the spectrum illuminating the disk can be ~ 5 times brighter than that emitted away from the disk (toward the observer; Ghisellini et al. 1991). This boosts the reflection component up to a maximum of $N_{refl} \sim 8$, sufficient to account for the hardest spectra seen in NGC 5548. This anisotropy can occur only if the soft photons from the disk are not first scattered by the cooled pairs in the source, which

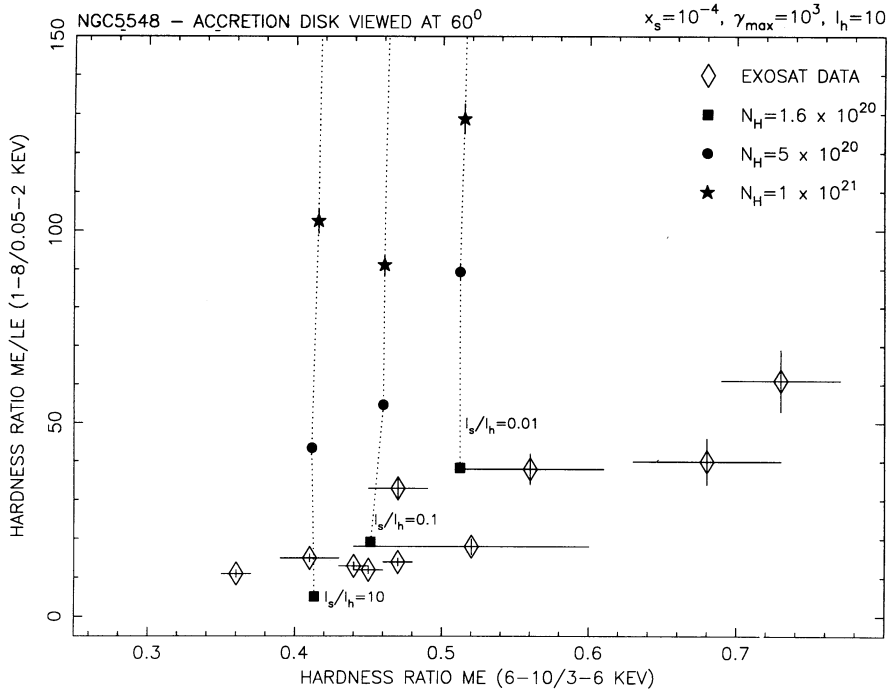

FIG. 8.—Predicted hardness ratios for absorption by increasing column density of cold gas: $N_H = 1.6 \times 10^{20}$, 5×10^{20}, and 1×10^{21} cm^{-2}. The input x_s and γ_{max} pair-reflection parameters are $x_s = 10^{-4}$, $\gamma = 10^3$, $N_{ref} = 1$, $l_s/l_h = [0.01, 0.1, 10]$ and $l_h = 10$. Increasing the column of cold absorbing gas makes the agreement between models and data even worse.

reisotropizes the distribution. This requires that the source have $\tau_T \leq 1$, i.e., that the hard compactness be low ($l_h \leq 10$). The hardest observed spectra tend to occur when the AGN is faint, so a possible scenario is that a low compactness state allows substantial anisotropy of the disk emission, enhancing the reflected Compton component. When the hard compactness increases, the source becomes optically thick and the soft photons scatter within the source before interacting with the relativistic electrons, suppressing the anisotropy so that the reflection normalization goes back to the expected value of $N_{refl} \leq 1.5$.

Variations in the column density of cold absorbing gas affect the hardness ratios but not in a way that explains the data. Figure 8 shows the dependence of the predicted hardness ratios on column density for $x_s = 10^{-4}$, $\gamma_{max} = 10^3$, $l_s/l_h = 0.01$, 0.1, 1, and $l_h = [2, 20, 200]$. The cold absorber decreases the LE flux,

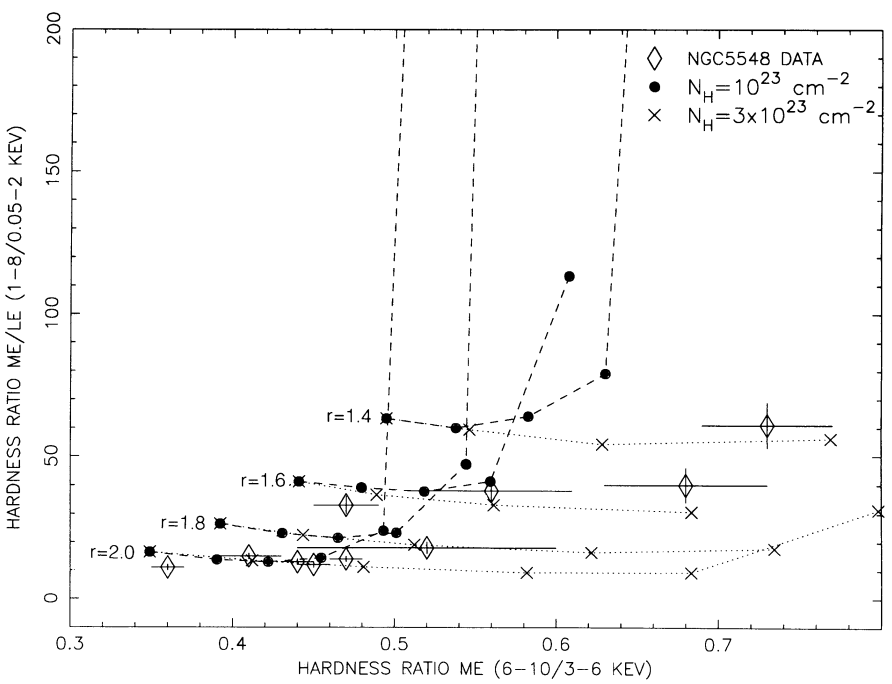

FIG. 9.—The effect of a warm ionized absorber for different power-law spectra with photon indeces 1.4, 1.6, 1.8, and 2.0. A very thick, highly ionized absorber ($N_H > 10^{23}$ cm^{-2}) can reproduce the hardest spectra of NGC 5548 even without a reflected component.

moving the points still higher in $HR_{ME/LE}$, and exacerbating the discrepancy between model and data. In any case, substantial amounts of cold absorbing material in the source were excluded by our selection criteria (see § 2).

On the other hand, partially ionized absorbers leave a soft excess (implying a lack of cold absorption) and affect the spectrum only at higher energies. The presence of a warm absorber has been suggested in several AGNs, where spectral variability appears to be caused by changes of the ionization state of warm gas located near the source (Halpern 1984; Pan, Stewart, & Pounds 1990; Nandra et al. 1991b; Yaqoob & Warwick 1991; Nandra & Pounds 1992; Nandra et al. 1993). Figure 9 shows the effect of partially ionized absorption on an incident power-law spectrum compared to the *EXOSAT* data for NGC 5548. The amount of absorption is determined both by the column density, N_H, and by the ionization state, here characterized by the ionization parameter $\xi = L/nr^2$, where n is the density of the material at distance r from the X-ray illuminating source of total luminosity L integrated between 5 eV and 300 keV (estimated in the present case from a simple extrapolation of the power-law flux). The hardness ratio changes with ionization, and for a given photon index and N_H, shows a characteristic curve, falling very steeply in $HR_{ME/LE}$ and then flatting out, moving to lower HR_{ME} as the ionization increases. The turning point in these curves is determined mainly by the oxygen abundance: when oxygen is largely unionized the gas effectively absorbs the LE flux, but if it is mostly ionized the LE flux passes freely through the gas. A column of $N_H \sim 10^{23}$ cm^{-2} has some effect on the 3–6 keV flux through absorption by Fe L-shell, and Si and S K-shell electrons, so the effect of increasing the ionization is to decrease the number of these species and so move points to lower values of HR_{ME}. Increasing the column to 3×10^{23} cm^{-2} drastically increases the effect on the 3–6 keV, and such a highly ionized, thick absorber can reproduce the hard spectra in NGC 5548 even without a nominal amount of reflection; however, this is much greater than the (admittedly very uncertain) column density inferred from *ROSAT*, *EXOSAT*, and *Ginga* data (Nandra et al. 1991b; Nandra et al. 1993).

6. CONCLUSIONS

Our results point to serious problems with interpreting the X-ray spectra of AGNs, notably *Ginga* spectra, with simple pair-reflection models. The additional information at soft energies available with the *EXOSAT* data reveals a range of spectral variability that is not reproduced by these models, even with a considerable range of input model parameters. None of the AGNs in our sample can be fitted by simply varying the hard compactness, in agreement with the conclusions of Yaqoob (1992) for NGC 4151. Even varying both l_s/l_h and l_h fails to explain the hardest HR_{ME} spectra in NGC 5548, NGC 7469, and 3C 120. It is possible that the single-source model can survive if the effects of anisotropic Compton illumination of the accretion disk are included, but this requires a detailed calculation which we have not attempted. Additional *external* components such as blackbody photons not intercepted by the source, enhanced reflection from material at large distances from the source (e.g., the molecular torus), or an ionized absorber can also reproduce the variability behavior. These alternative scenarios can be tested easily with multiwavelength monitoring. Anisotropic reflection from the accretion disk will produce large changes in hard X-ray flux which should be quasi-simultaneous (as the accretion disk length is probably less than a few light hours) with smaller changes in the soft X-ray flux, whereas reflection from the torus predicts that the hard (reflected) photons should lag the softer (direct) photons by a considerable amount, related to the dimensions of the torus (light-days to eight-months). In the event that the variability is caused by a partially ionized absorber, particularly one where oxygen is partially ionized, strong and variable X-ray spectral features should be visible in the moderate-resolution ASCA spectra. In any case, in order for the pair-reflection model to remain viable, the observed spectral variability must be largely affected by external factors rather than by the pairs and reflection processes themselves.

We thank Ian George for providing a ASCII-binary conversion code for the ATABLE package in XSPEC, Lorella Angelini for the *EXOSAT* database assistance, and Mauro Giavalisco for very useful FORTRAN suggestions. We are also very grateful to Paolo Coppi and Greg Madejski for helpful discussions and to the anonymous referee for useful comments. We are particularly grateful to Paolo Coppi for providing some spectra from his code, allowing us to estimate the effects of our computation approximations. P. G. and C. M. U. acknowledge the financial support from the ST ScI collaborative visitor program, which allowed the start of this work, and from NASA grant NAG8-697.

REFERENCES

Arnaud, K. A., et al. 1985, MNRAS, 217, 105
Barr, P. 1986, MNRAS, 223, 29P
Branduardi-Raymont, G. 1986, in The Physics of Accretion onto Compact Objects, ed. K. O. Mason, M. G. Watson, & N. E. White (Berlin: Springer-Verlag), 407
Coppi, S. P., & Zdziarski, A. A. 1992, ApJ, 398, L37
Courvoisier, T. J. L., & Camenzind, M. 1989, A&A, 224, 10
Done, C., & Fabian, A. C. 1989, MNRAS, 240, 81
Done, C., Ghisellini, G., & Fabian, A. C. 1990, MNRAS, 245, 1
Fabian, A. C., et al. 1986, MNRAS, 221, 931
Fiore, F., Perola, G. C., Matsuoka, M., Yamauchi, M., & Piro, L. 1992, A&A, 262, 37
George, I. M., & Fabian, A. C. 1990, MNRAS, 249, 352
Ghisellini, G., George, I. M., Fabian, A. C., & Done, C. 1991, MNRAS, 248, 14
Grandi, P., Tagliaferri, G., Giommi, P., Barr, P., & Palumbo, G. G. C. 1992, ApJS, 82, 93 (G92)
Guilbert, P. W., Fabian, A. C., & Rees, M. J. 1983, MNRAS, 205, 593
Guilbert, P. W., & Rees, M. J. 1988, MNRAS, 233, 475
Haardt, F. 1993, ApJ, 413, 680
Halpern, J. P. 1984, ApJ, 281, 90
Kaastra, J., & Barr, P. 1989, A&A, 226, 59
Kazanas, D. 1984, ApJ, 287, 112
Kruper, J. S., Urry, C. M., & Canizares, C. R. 1990, ApJS, 74, 347
Laor, A. 1990, MNRAS, 246, 369
Lawrence, A. 1991, MNRAS, 252, 586
Leighly, K. M., Pounds, K. A., & Turner, T. J. 1989, in X-Ray Astronomy, Proc. of the 23rd ESLAB Symp., ed. N. E. White, Vol. 2, 961
Lightman, A. P., & White, T. R. 1988, ApJ, 335, 57
Lightman, A. P., & Zdziarski, A. A. 1987, ApJ, 319, 643
Maisack, M., & Yaqoob, T. 1991, A&A, 249, 25
Maisack, M., et al. 1992, A&A, 262, 433
———. 1993, ApJ, 407, L61
Maraschi, L., Chiappetti, L., Falomo, R., Garilli, B., Malkan, M., Tagliaferri, G., Tanzi, E. G., & Treves, A. 1991, ApJ, 361, 440
Matt, G., Perola, G. C., & Piro, L. 1991, A&A, 247, 25
McHardy, I. 1989, in X-Ray Astronomy, Proc. of the 23rd ESLAB Symp., ed. N. E. White, Vol. 2, 1111
Nandra, K., et al. 1993, MNRAS, 260, 504
Nandra, K., & Pounds, K. A. 1992, Nature, 359, 215
Nandra, K., Pounds, K. A., & Stewart, G. C. 1991a, in Iron Line Diagnostics in X-ray Sources, ed. A. Treves, G. C. Perola, & L. Stella (Berlin: Springer-Verlag), 177
Nandra, K., Pounds, K. A., Stewart, G. C., George, I. M., Hayashida, K., Makino, F., & Ohashi, T. 1991b, MNRAS, 248, 760
Pagel, B. E. J., & Edmunds, M. G. 1981, ARA&A, 19, 77
Pan, H. C., Stewart, G. C., & Pounds, K. A. 1990, MNRAS, 242, 177

Piccinotti, G., Mushotzky, R. F., Boldt, E. A., Holt, S. S., Marshall, F. E., Serlemitsos, P. J., & Shafer, R. A. 1982, ApJ, 253, 485
Piro, L., Yamauchi, M., & Matsuoka, M. 1990, ApJ, 360, L35
Pounds, K. A., Nandra, K., Stewart, G. C., & Leighly, K. 1989, MNRAS, 240, 769
Pounds, K. A., et al. 1990, Nature, 344, 132
Pozdnyakov, L. A., Sobol, I. M., & Sunyaev, R. A. 1983, in Soviet Sci. Rev. Ap. & Space Phys., 2, 189
Ross, R., & Fabian, A. C. 1993, MNRAS, 261, 74
Rogers, R. D. 1991, ApJ, 383, 550
Stark, A. A., et al. 1992, ApJS, 79, 77
Staubert, R., Fink, H., Courvoisier, T. J. L., Ulrich, M. H., Brunner, H., Zimmermann, U., Kendziorra, E., & Otterbein, K. 1991, in Testing the AGN Paradigm, ed. S. S. Holt, S. J. Neff, & C. M. Urry (New York: AIP), 366
Sunyaev, R. A., & Titarchuk, L. G. 1980, A&A, 86, 121
Svensson, R. 1987, MNRAS, 227, 403
———. 1991, in X-ray Emission from AGN and the Cosmic X-ray Background, ed. W. Brinkmann & J. Trumper (Garching-bei-München: MPE), 103
Turner, M. J. L., et al. 1990, MNRAS, 244, 310
Turner, T. J., & Pounds, K. A. 1989, MNRAS, 240, 833
Turner, T. J., et al. 1993, ApJ, 407, 556
Urry, C. M., Arnaud, K. A., Edelson, R. A., Kruper, J. S., & Mushotzky, R. F. 1989, in AGN and the X-Ray Background, ed. N. E. White (ESA SP 296), 789
Walter, R., & Courvoisier, T. J. L. 1990. A&A, 233, 40
Wandel, A., & Mushotzky, R. F. 1986, ApJ, 306, L61
White, T. R., Lightman, A. P., & Zdziarski, A. A. 1988, ApJ, 331, 939
Wilkes, B. J., & Elvis, M. 1987, ApJ, 323, 243
Williams, O. R., et al. 1992, ApJ, 389, 157
Worral, D. M., et al. 1979, ApJ, 232, 683
Yaqoob, T. 1992, MNRAS, 258, 198
Yaqoob, T., & Warwick, R. S. 1991, MNRAS, 248, 773
Yaqoob, T., et al. 1993, MNRAS, 262, 435
Zdziarski, A. A. 1986, ApJ, 305, 45
———. 1988, ApJ, 335, 786
Zdziarski, A. A., & Coppi, P. S. 1991, ApJ, 376, 149
Zdziarski, A. A., Coppi, P. S., & Lamb, D. Q. 1990b, ApJ, 357, 149
Zdziarski, A. A., Ghisellini, G., George, I. M., Svensoon, R., Fabian, A. C., & Done, C. 1990a, ApJ, 363, 45
Zdziarski, A. A., & Lightman, A. P. 1985, ApJ, 294, L79
Zdziarski, A. A., Lightman, A. P., & Maciolek-Niedzwiecki, A. 1993, ApJ, in press